# Multilevel light-induced continuum structure: Strong-probe and stabilization effects

R. Parzyński, A. Wójcik, and J. Schmidt

*Quantum Electronics Laboratory, Institute of Physics, A. Mickiewicz University, Grunwaldzka 6, 60-780 Poznań, Poland*

We present an analytical solution to a multilevel model of light-induced continuum structure, in which, instead of a single level, a quasicontinuum of excited levels is laser embedded into a previously structureless atomic continuum. The found solution is fully time dependent and is valid for probing strengths of the structured continuum from the ground level by another laser, which can vary from being much weaker than the embedding one to being as strong as the embedding one. For three different embeddings (weak, moderate, and strong), each one determined by a different relation between the ionization rate $\gamma$ and the spacing $\Delta$ of the quasicontinuum levels ($\hbar\gamma/\Delta \ll 1$, $\hbar\gamma/\Delta \simeq 1$, and $\hbar\gamma/\Delta \gg 1$), we study the evolution of the ionization spectrum with increasing probing strength. We observe and interpret such strong-field effects in the spectra as (i) conversion of a Fano-like train of peaks into a train of dips; (ii) peak moving, narrowing, and lowering; and (iii) saturation, population trapping, and stabilization against ionization.

PACS number(s): 32.80.Rm, 42.50.Hz

## I. INTRODUCTION

In its fundamental formulation [1], the model of what is termed a light-induced continuum structure (LICS) involves only a pair of discrete levels (the ground and an excited), which are Raman coupled via structureless continuum by the use of two separate lasers. The strong laser, embedding the excited level into the continuum, is known to dress this continuum introducing some structure into it with the position and width of this structure depending on the embedding-laser frequency and intensity. If such a structured continuum is probed from the ground level by a weak laser, it usually gives a resonant-like profile when measuring ionization versus probe-laser frequency. Asymmetry of this profile is what is traditionally considered as evidence of LICS. However, it has been known since 1986 [2–4] that under the LICS conditions a supplementary Raman coupling between the two discrete levels of the LICS model, i.e., the coupling that employs non-resonant bound states of real atom as an intermediary, plays its role as well. The effect of this additional coupling is to symmetrize the profile and thus to mask the pure LICS effect. Now we know that not only this additional coupling, but also realistic atomic parameters and the actual spatiotemporal characteristics of the lasers [5], as well as continuum-continuum transitions [6], must in general be taken into account to explain the LICS phenomenon. As a comprehensive review article on a LICS is available we refer the reader to it [7] instead of quoting a number of papers discussing a LICS in a variety of contexts, e.g., the context of optical-polarization rotation, third-harmonic generation, frequency up-conversion, multiphoton ionization, photoelectron-spin polarization, population trapping, and control of ionization rates. Though known for many years, the LICS has achieved direct experimental evidence in ionization only very recently. At the end of 1991 two groups did report the observation of a LICS in

atomic sodium [8,9]. In both experiments the ground level was that from which the structured continuum was probed. Depending on the experiment, the excited level embedded into the continuum was either $4S$ or $5S$. Both experiments consisted in measuring the ionization signal versus the frequency of the probe laser and in both a substantially asymmetric profile was actually observed. In the middle of 1993 one of these groups [10] reported direct observation of a LICS in ionization of calcium atoms where real autoionizing states contributed essentially to the effect. Quite recently the possibility of observing a LICS in multiphoton detachment of the electron from negative ions was contemplated [11], and in [12] an analog of a LICS in photonic continuum was considered.

It is rather a simple task to point out the situations in which the fundamental model of a LICS is expected not to work well. One such a situation is when the excited level has some internal structure or it is in the company of another close-lying level. In fact, the model of a LICS with a pair of excited levels, dictated by the appropriate experiment [2], was worked out by us [13] and shown to give a richer ionization spectrum. The extreme seems to be the case when a highly excited level lying close to the ionization edge is laser embedded into continuum. Because of high density of levels in this region, their ionization broadening, and finite bandwidth of the laser, the term "isolated level" bears no sense any longer. In this case it is adequately to speak about a group of levels, forming some type of quasicontinuum, being laser embedded into continuum. Such a multilevel model of a LICS was recently introduced by us [14] and solved, but only in the limiting case of a weak probe. At present, we give and discuss general solution of our multilevel LICS problem, nonperturbative with respect to both laser intensities, the solution which also covers the case when probing is as strong as embedding. The advantage of the general solution presented is its completely analytical form. Ob-

viously, to achieve such an analytical solution we had to make a number of approximations. The most important of them concerns modeling of the embedded quasicontinuum by the Bixon-Joertner structure (e.g., [15–19]). Though an idealization, the Bixon-Joertner quasicontinuum is often considered as a good first approach to any real quasicontinuum, particularly of Rydberg type in the so-called semiclassical region [20]. Thus the results, though obtained within the model, are believed to have a correspondence to real atomic objects. Another important approximation is that of rectangular-in-time optical pulses, which we have made in fact, though we are aware of the role of the pulse shape in the interpretation of experimental spectra of the LICS [5]. These two approximations, when put together with the rotating-wave approximation (RWA), pole approximation, and semiclassical approximation for bound-free matrix elements, have made our multilevel model of the LICS analytically solvable for arbitrary laser pulse intensities and durations.

Our paper is organized as follows. In Sec. II we present formal theory. Section II A is devoted to introducing our general model, called the $N$-type model, and solving it completely in the Laplace domain. Then this solution is specialized In Sec. II B to a simpler model of $\Lambda$ type, obtained from the previous one by ignoring one of the two atomic continua originally included. In Sec. II C we present analytical time-dependent amplitudes for all levels of our $\Lambda$ model, obtained by adopting the Bixon-Joertner quasicontinuum. Our representative results are then given and discussed in Sec. III, with emphasis on strong-probe and stabilization effects. We end our paper with a summary in Sec. IV.

## II. THEORY

### A. General $N$-type model

The essence of our model (Fig. 1) is a stimulated Raman transition between a low-lying isolated discrete level, to be referred to as the ground level, and a set of high-lying closely spaced discrete levels forming some type of
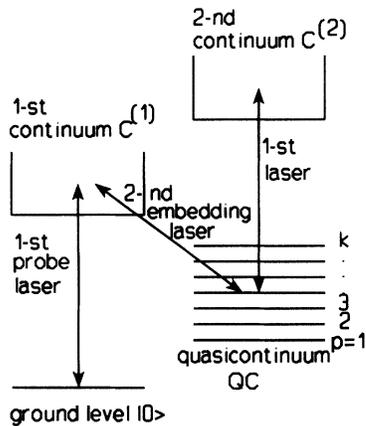


FIG. 1. General $N$-type atomic model of a LICS with a quasicontinuum of excited levels QC, and two continua $C^{(1)}$ and $C^{(2)}$.

quasicontinuum (QC). This Raman transition is assumed to be accomplished by two independent laser pulses employing the structureless atomic continuum ($C$) as an intermediary. Obviously, another intermediary formed of the off-resonant bound states lying below ionization threshold should in general be considered as well when two lasers are applied [2–7]. Since the effect of this additional intermediary is only to redefine [3,4] the appropriate Fano parameters, to be introduced later on, we have decided not to reveal it in Fig. 1. The laser pulses are assumed to be overlapping in time and we idealize them as having a rectangular time envelope. We attach the index 0 to the ground level and indices $p = 1,2,\ldots,k$ to the levels in the QC, allowing $k$ to tend to infinity in the extreme case. To save space, when writing down equations of motion, we also introduce the index $n$ encompassing all discrete levels of the model, i.e., such that $n = 0,1,2\ldots,k$ ($\{n\} = \{0,\{p\}\}$). We shall call the continuum playing the role of the intermediary in the Raman transition as the first continuum and label it by $C^{(1)}$. It is obvious that another second continuum $C^{(2)}$, reached from the QC by the first probe laser, must in general be included as well. With this additional continuum taken into account, our model is of $N$ type rather than $\Lambda$ type, with $C$-$C$ transitions ignored. We also ignore the effect of the second embedding laser on the ground level to continuum coupling. To have the results obtained within this model as general as possible, we do not specify at the beginning which discrete level of the model is initially, i.e., at $t = 0$, occupied.

Let $\tilde{b}_n$ be the Laplace transforms of population amplitudes of discrete levels of the model, while $\tilde{b}_{E^{(1)}}$ and $\tilde{b}_{E^{(2)}}$ are those of the first and the second continuum, respectively. In the RWA these amplitudes are to be found from the Laplace form of the Schrödinger equation

$$\left(s+i\frac{E_\alpha}{\hbar}\right)\tilde{b}_\alpha = (i\hbar)^{-1}\sum_\beta V_{\alpha\beta}\tilde{b}_\beta + b_\alpha(0) , \tag{1}$$

where $s$ is the Laplace variable, $b_\alpha(0)$ is the value of the amplitude at $t = 0$, $V_{\alpha\beta}$ is the matrix element of the atom-laser interaction, and $E_\alpha$ denotes the energy of the combined atom plus the laser-field state with the field described in photon-number language. For our $N$-type model this equation splits into

$$\left(s+i\frac{E_n}{\hbar}\right)\tilde{b}_n = b_n(0)+(i\hbar)^{-1}\sum_{E^{(1)}} V_{nE^{(1)}}\tilde{b}_{E^{(1)}}$$
$$+\Theta(n)(i\hbar)^{-1}\sum_{E^{(2)}} V_{nE^{(2)}}\tilde{b}_{E^{(2)}} , \tag{2}$$

$$\left(s+i\frac{E^{(1)}}{\hbar}\right)\tilde{b}_{E^{(1)}} = (i\hbar)^{-1}\sum_{n=0}^{k} V_{E^{(1)}n}\tilde{b}_n , \tag{3}$$

$$\left(s+i\frac{E^{(2)}}{\hbar}\right)\tilde{b}_{E^{(2)}} = (i\hbar)^{-1}\sum_{n=0}^{k} \Theta(n)V_{E^{(2)}n}\tilde{b}_n , \tag{4}$$

with $\Theta(n)$ being the discrete Heaviside function defined as $\Theta(n = 0) = 0$ and $\Theta(n = p) = 1$ for all $1 \le p \le k$. As is

traditional, we remove the continuum state amplitudes $\tilde{b}_{E^{(1)}}$ and $\tilde{b}_{E^{(2)}}$ from Eq. (2) by substituting into it Eqs. (3) and (4) and then replacing the sums over continuum states by energy integrals $[\sum_E \rightarrow \int d(E)dE]$, assuming for simplicity the same state density in both continua $[d(E^{(1)})=d(E^{(2)})=d]$. After the standard pole approximation, Eq. (2) is converted into the equation for discrete-state amplitudes only:

$$\left[s+i\frac{E_n}{\hbar}\right]\tilde{b}_n + \frac{\pi}{\hbar}d\sum_{n'=0}^{k}(1+iq_{nn'}^{(1)})V_{nE^{(1)}}V_{E^{(1)}n'}\tilde{b}_{n'}$$

$$+\frac{\pi}{\hbar}d\Theta(n)\sum_{n'=0}^{k}\Theta(n')(1+iq_{nn'}^{(2)})V_{nE^{(2)}}V_{E^{(2)}n'}\tilde{b}_{n'}=b_n(0)$$

$$(5)$$

in which

$$q_{nn'}^{(i)} = \frac{\left[-P\int\left[\frac{V_{nE^{(i)}}V_{E^{(i)}n'}}{E^{(i)}}\right]d(E^{(i)})dE^{(i)}\right]}{\pi V_{nE^{(i)}}V_{E^{(i)}n'}d(E^{(i)})} \quad (6)$$

is a Fano parameter [7] for the coupling between any two discrete levels via the continuum $(i=1,2)$.

Having obtained Eq. (5), we apply it to calculate the continuum-state population amplitudes from Eqs. (3) and (4). According to these equations, we need to find two sums

$$\sum_{n=0}^{k}V_{E^{(1)}n}\tilde{b}_n = V_{E^{(1)}0}\tilde{b}_0 + \sum_{p=1}^{k}V_{E^{(1)}p}\tilde{b}_p , \quad (7)$$

$$\sum_{n=0}^{k}\Theta(n)V_{E^{(2)}n}\tilde{b}_n = \sum_{p=1}^{k}V_{E^{(2)}p}\tilde{b}_p , \quad (8)$$

in which we have split the discrete-level space into the ground-level and the QC-level subspaces. For these two subspaces we get from Eq. (5)

$$\left[s+i\frac{E_0'}{\hbar}+\frac{\gamma_0}{2}\right]\tilde{b}_0$$

$$+\frac{\pi}{\hbar}dV_{0E^{(1)}}\sum_{p'=1}^{k}(1+iq_{0p'}^{(1)})V_{E^{(1)}p'}\tilde{b}_{p'}=b_0(0) , \quad (9)$$

$$\left[s+i\frac{E_p}{\hbar}\right]\tilde{b}_p + \frac{\pi}{\hbar}d(1+iq_{p0}^{(1)})V_{pE^{(1)}}V_{E^{(1)}0}\tilde{b}_0$$

$$+\frac{\pi}{\hbar}dV_{pE^{(1)}}\sum_{p'=1}^{k}(1+iq_{pp'}^{(1)})V_{E^{(1)}p'}\tilde{b}_{p'}$$

$$+\frac{\pi}{\hbar}dV_{pE^{(2)}}\sum_{p'=1}^{k}(1+iq_{pp'}^{(2)})V_{E^{(2)}p'}\tilde{b}_{p'}=\tilde{b}_p(0) , \quad (10)$$

where

$$E_0'-E_0=\pi dq_{00}^{(1)}|V_{0E^{(1)}}|^2$$

$$=-P\int(|V_{0E^{(1)}}|^2/E^{(1)})d(E^{(1)})dE^{(1)}$$

and $\gamma_0=(2\pi/\hbar)|V_{0E^{(1)}}|^2d$ are the shift and the width of the ground level due to its coupling to the first continuum

by the first laser. Formally, we treat Eqs. (9) and (10) as a set which is to be solved with respect to $\tilde{b}_0$ and $\tilde{b}_p$. We calculate $\tilde{b}_0$ from Eq. (9) and then insert it into Eq. (10), obtaining, as a result, the equation for QC levels only. As required by Eqs. (7) and (8), we multiply the obtained equation by $V_{E^{(i)}p}$ and sum it over all $p$. Though in general the sum $\sum_p V_{E^{(i)}p}\tilde{b}_p$ cannot be found in a close form, there fortunately is the case when it can be done. From now on we shall exclusively focus on this case, which is defined by the approximations

$$q_{p0}^{(1)}=q_{0p}^{(1)}=q \neq f(p) ,$$

$$q_{pp'}^{(1)}=q_{p'p}^{(1)}=q^{(1)}\neq f(p,p') ,$$

$$q_{pp'}^{(2)}=q_{p'p}^{(2)}=q^{(2)}\neq f(p,p') , \quad (11)$$

$$\frac{|V_{E^{(2)}p}|^2}{|V_{E^{(1)}p}|^2}=\frac{\gamma_p^{(2)}}{\gamma_p^{(1)}}=\eta\neq f(p) ,$$

where $\eta$ is the branching ratio for ionization from a given QC level to the two continua allowed $[\gamma_p^{(i)}=(2\pi/\hbar)|V_{pE^{(i)}}|^2d]$. The case defined by Eqs. (11) means that this branching ratio is approximated to be $p$ independent, i.e., the same for all QC levels. It also means that the Raman coupling between the ground level and the QC is governed by one Fano parameter $q$, also $p$ independent. This $p$ independence is also maintained for the Raman coupling between any two QC levels via the first continuum $(q^{(1)})$ and via the second continuum $(q^{(2)})$. Obviously, these approximations are restrictive, but are roughly justified, e.g., for a highly excited Rydberg QC since then the matrix elements depend only on the appropriate power of the QC index $(p^{-3/2})$. With these approximations, the sum required is found to be

$$\sum_{p=1}^{k}V_{E^{(1)}p}\tilde{b}_p = \frac{p(s)-f(s)Q(s)b_0(0)}{1+f(s)R(s)}=S(s) , \quad (12)$$

where

$$p(s)=\sum_{p'=1}^{k}\frac{V_{E^{(1)}p'}b_{p'}(0)}{s+i\frac{E_{p'}}{\hbar}} , \quad (13)$$

$$f(s)=\sum_{p'=1}^{k}\frac{\gamma_p^{(1)}/2}{s+i\frac{E_{p'}}{\hbar}} , \quad (14)$$

$$Q(s)=\frac{(1+iq)V_{E^{(1)}0}}{s+i\frac{E_0'}{\hbar}+\frac{\gamma_0}{2}} , \quad (15)$$

$$R(s)=\frac{\alpha\left[s+i\frac{E_0'}{\hbar}\right]+\beta}{s+i\frac{E_0'}{\hbar}+\frac{\gamma_0}{2}} , \quad (16)$$

with

$$\alpha=1+\eta+i(q^{(1)}+\eta q^{(2)}) , \quad (17)$$

$$\beta=[\alpha-(1+iq)^2]\frac{\gamma_0}{2} \ . \tag{18}$$

The noteworthy fact is that the sum $S(s)$ is a function of only the atom-laser coupling matrix elements and the initial conditions, with no population amplitude involved. This $S(s)$, along with the approximations (11), gives the appropriate $\tilde{b}_0$ from Eq. (9). Having $\tilde{b}_0$, we find $\tilde{b}_p$ from Eq. (10). With $\tilde{b}_0$ and $S(s)$ available, we recall Eqs. (3) and (4) and calculate $\tilde{b}_{E^{(1)}}$ and $\tilde{b}_{E^{(2)}}$ from them. Along this line, our starting Laplace equations of motion [Eqs. (2)–(4)] are found to have solutions in the form

$$\tilde{b}_0=\frac{1}{D(s)}\left\{[1+\alpha f(s)]b_0(0)\right.$$
$$\left.-\frac{\pi}{\hbar}d(1+iq)V_{0E^{(1)}}p(s)\right\} , \tag{19}$$

$$\tilde{b}_p=\frac{1}{s+i\dfrac{E_p}{\hbar}}\left\{b_p(0)-\frac{\dfrac{\pi}{\hbar}dV_{pE^{(1)}}}{D(s)}\right.$$
$$\times\left\{(1+iq)V_{E^{(1)}0}b_0(0)\right.$$
$$+\left[\alpha\left(s+i\frac{E_0'}{\hbar}\right)+\beta\right]$$
$$\left.\left.\times p(s)\right\}\right\} , \tag{20}$$

$$\tilde{b}_{E^{(1)}}=\frac{(i\hbar)^{-1}}{s+i\dfrac{E^{(1)}}{\hbar}}\frac{1}{D(s)}$$
$$\times\left\{[1+(\alpha-1-iq)f(s)]V_{E^{(1)}0}b_0(0)\right.$$
$$+\left.\left[s+i\frac{E_0}{\hbar}\right]p(s)\right\} , \tag{21}$$

$$\tilde{b}_{E^{(2)}}=\frac{-(i\hbar)^{-1}}{s+i\dfrac{E^{(2)}}{\hbar}}\frac{\sqrt{\eta}}{D(s)}\left\{(1+iq)V_{E^{(1)}0}f(s)b_0(0)\right.$$
$$-\left.\left[s+i\frac{E_0'}{\hbar}+\frac{\gamma_0}{2}\right]p(s)\right\} , \tag{22}$$

where

$$D(s)=s+i\frac{E_0'}{\hbar}+\frac{\gamma_0}{2}+\left[\alpha\left(s+i\frac{E_0'}{\hbar}\right)+\beta\right]f(s) \ . \tag{23}$$

### B. Simplified Λ model

From now on we shall concentrate on a simplified version of our model when the first probe laser is weak when compared to the second embedding one. This means that

the second continuum reached from the QC by the first laser is only poorly populated and, as a result, can be neglected to a good approximation ($\eta=0$). The model simplified in such a way is thus of Λ type (Fig. 2). This one-continuum model does not necessarily imply that the ground level is coupled more weakly to the continuum than the QC levels. This is so because, besides laser intensity, the other factor influencing the strength of coupling is the dipole matrix element which, for realistic levels, diminishes drastically with increasing level index. It is thus likely that a highly excited QC can be coupled even more weakly to the continuum by the strong second laser than the ground level is coupled to the continuum by the weak first laser. We also take the liberty of setting the Fano parameters identical ($q=q^{(1)}=q^{(2)}$). With these two assumptions, $\alpha$ and $\beta$ defined by Eqs. (17) and (18) become proportional to each other, namely, $\beta=-iq\gamma_0(\alpha/2)$, where now $\alpha=1+iq$. This proportionality relation implies considerable simplification of our general Laplace solution, given by Eqs. (19)–(23), to the form

$$\tilde{b}_n=-\frac{1}{s+i\dfrac{E_n}{\hbar}}\left\{b_n(0)-\frac{\pi}{\hbar}d(1+iq)\right.$$
$$\left.\times V_{nE^{(1)}}\frac{P(s)}{1+(1+iq)F(s)}\right\} , \tag{24}$$

$$\tilde{b}_{E^{(1)}}=\frac{(i\hbar)^{-1}}{s+i\dfrac{E^{(1)}}{\hbar}}\frac{P(s)}{1+(1+iq)F(s)} , \tag{25}$$

when $n$ encompasses both 0 ( ground level) and $p$ (QC levels), while

$$P(s)=\sum_{n'=0}^{k}\frac{V_{E^{(1)}n'}b_{n'}(0)}{s+i\dfrac{E_{n'}}{\hbar}} , \tag{26}$$

$$F(s)=\sum_{n'=0}^{k}\frac{\gamma_{n'}^{(1)}/2}{s+i\dfrac{E_{n'}}{\hbar}} \tag{27}$$

are generalizations, by inclusion of the ground level, of
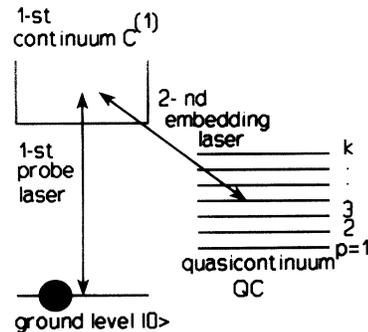


FIG. 2. Simplified Λ-type atomic model of a LICS with a quasicontinuum of excited levels QC and one continuum $C^{(1)}$. The population is initially in the ground level $|0\rangle$.

our previous functions $p(s)$ and $f(s)$ [see Eqs. (13) and (14)]. We would like to stress that by neglecting the first laser, and thus the ground level, along with setting $q=0$, Eqs. (24) and (25) are converted into those of Fedorov and Movsesian [21] for their model of one-laser coupling between Rydberg levels and continuum. With the ground level included in our two-laser $\Lambda$ model we will encounter a more troublesome problem of the transformation our Laplace solutions into time-dependent amplitudes.

As typical for the LICS, we now assume that initially at $t=0$ all the population is in the ground level $|0\rangle$. This means $b_n(0)=\delta_{n0}$, entailing $P(s)=V_{E^{(1)}0}/[s+i(E_0/\hbar)]$. In this case it turns out to be convenient to define the function

$$G(s)=\frac{1}{\left[s+i\dfrac{E_0}{\hbar}\right]^2}\frac{1}{1+(1+iq)F(s)} \qquad (28)$$

and to express through it all Laplace amplitudes with the results

$$\tilde{b}_0=\frac{1}{s+i\dfrac{E_0}{\hbar}}-(1+iq)\left[\frac{\gamma_0}{2}\right]G(s), \qquad (29)$$

$$\tilde{b}_p=-(1+iq)\left[\frac{\sqrt{\gamma_p\gamma_0}}{2}\right]\left\{G(s)+\frac{E_p-E_0}{i\hbar}\frac{G(s)}{s+i\dfrac{E_p}{\hbar}}\right\}, \qquad (30)$$

$$\tilde{b}_{E^{(1)}}=(i\hbar)^{-1}V_{E^{(1)}0}\left[G(s)+\frac{E^{(1)}-E_0}{i\hbar}\frac{G(s)}{s+i\dfrac{E^{(1)}}{\hbar}}\right]. \qquad (31)$$

As a consequence, the time-dependent amplitudes become

$$b_0(t)=e^{-iE_0t/\hbar}-(1+iq)\left[\frac{\gamma_0}{2}\right]G(t), \qquad (32)$$

$$b_p(t)=-(1+iq)\left[\frac{\sqrt{\gamma_p\gamma_0}}{2}\right]$$
$$\times\left[G(t)+\frac{E_p-E_0}{i\hbar}I(t,E_p)\right], \qquad (33)$$

$$b_{E^{(1)}}(t)=\frac{V_{E^{(1)}0}}{i\hbar}\left[G(t)+\frac{E^{(1)}-E_0}{i\hbar}I(t,E^{(1)})\right], \qquad (34)$$

where in accordance with the convolution theorem

$$I(t,\dot{E})=\int_0^t e^{i(t'-t)E/\hbar}G(t')dt', \qquad (35)$$

with $G(t)$ being the Laplace inversion of $G(s)$. As seen, only $G(t)$ and $I(t,E)$ are what we need. Obviously, $G(t)$ depends on the type of QC and we emphasize that only for a very special QC the analytical form of $G(t)$, and thus $I(t,E)$ as well, is possible to be found. Below, we shall proceed with one such QC.

### C. $\Lambda$ model with the Bixon-Joertner QC

The Bixon-Joertner QC is a very popular structure particularly in the theories of intramolecular processes [15], quasicontinuum photoexcitation [16–19], and Rydberg-atom stabilization in strong laser fields [20–23]. It is an infinite sequence of equidistant levels, with energy spacing $\Delta$, which are coupled to continuum with the same strength $\gamma$ independent of the QC index $p$. This QC imitates pretty well the realistic highly excited $(p\gg1)$ Rydberg QC, for which the energy spacing is $\Delta=2\mathcal{R}/p^3$ and the coupling to continuum behaves like $\gamma\sim1/p^3$ in the so-called semiclassical region [20]. As long as $|p-p^{(0)}|\ll p^{(0)}$, where $p^{(0)}$ is some central level in the Rydberg QC, the two parameters $\Delta$ and $\gamma$ are practically the same for all $p$, justifying the introduction of the Bixon-Joertner structure. For the Bixon-Joertner QC the function $F(s)$, defined by Eq. (27) and inherent in Eq. (28) for $G(s)$, is recast to

$$F(s)=\frac{\gamma_0/2}{s+i\dfrac{E_0}{\hbar}}+\frac{\gamma}{2}\frac{\pi}{\Delta/\hbar}\coth\left[\frac{\pi}{\Delta/\hbar}\left[s+i\frac{E^{(0)}}{\hbar}\right]\right], \qquad (36)$$

where $E^{(0)}$ is the energy of the central level in the QC combined with laser-field energy $(E_p=E^{(0)}+p\Delta)$.

To invert $G(s)$, we follow the method of Stey and Gibberd [24], i.e., we use the exponential representation $\coth(x)=(1+\alpha)/(1-\alpha)$, with $\alpha=e^{-2x}$, and expand $G(s)$ in powers of $\alpha$ applying the relation

$$\frac{1}{a+b\coth(x)}=\frac{1}{a+b}-2b\sum_{m=1}^{\infty}\frac{(a-b)^{m-1}}{(a+b)^{m+1}}\alpha^m. \qquad (37)$$

After this, we make use of the inversion formula [17,25]

$$\frac{(s-\lambda-\beta)^{m-1}}{(s-\lambda)^{m+1}}\rightarrow\frac{1}{m}te^{\lambda t}L_{m-1}^1(\beta t), \qquad (38)$$

where $L_q^1$ is an associated Laguerre polynomial. The required $G(t)$ is then found in a completely analytical form as

$$G(t)=\frac{e^{-iE_0t/\hbar}}{(1+iq)\gamma_0/2}[1-e^{-2\pi\rho\tau}-(2\pi)^2uvZ(\tau)], \qquad (39)$$

where

$$Z(\tau)=\sum_{m=1}^{\infty}(\tau-m)A_m(\tau)L_{m-1}^1(\beta(\tau-m))\Theta(\tau-m) \qquad (40)$$

with $\beta=-4\pi^2uv/[1-(\pi v)^2]$. Here $\Theta(\tau-m)$ is Heaviside function, being nonzero (equal to 1) only for $\tau-m>0$, while

$$A_m(\tau)=\frac{(1-\pi v)^{m-1}}{(1+\pi v)^{m+1}}\frac{e^{-i2\pi mx}}{m}e^{-2\pi\rho(\tau-m)}, \qquad (41)$$

$$L_{m-1}^1(\beta(\tau-m))=\sum_{j=0}^{m-1}\alpha_j(m)(\tau-m)^j, \qquad (42)$$

$$\alpha_j(m)=\frac{(2\pi)^{2j}}{j!}\left[\begin{matrix}m\\m-j-1\end{matrix}\right]\left[\frac{\rho v}{1-\pi v}\right]^j, \qquad (43)$$

and

$$\rho = \frac{u}{1+\pi v}, \quad u = \frac{(1+iq)\gamma_0/2}{\Delta/\hbar}, \quad v = \frac{(1+iq)\gamma/2}{\Delta/\hbar},$$

$$x = \frac{E^{(0)} - E_0}{\Delta} = \frac{\delta}{\Delta/\hbar}, \quad \tau = \frac{t}{2\pi\hbar/\Delta} = \frac{t}{t_r}. \quad (44)$$

The parameters $u$ and $v$ are the measures of the ground-level coupling strength and the QC-coupling strength to the continuum, respectively, $\delta$ is the detuning from two-photon Raman resonance between the ground level and the central level in the QC, and $t_r = 2\pi\hbar/\Delta$ is the so-called recurrence time. For the highly excited Rydberg QC, this time coincides with the classical Kepler time of the orbiting electron $t_r = t_K = (\pi\hbar/\mathcal{R})p^3$, with $p$ having the sense of the principal quantum number.

Having calculated $G(t)$, we are able to find the needed integral $I(t,E)$ defined by Eq. (35). Thanks to the power-in-$\tau$ representation of Laguerre polynomial [Eq. (42)] we readily obtain

$$I(t,E) = -\frac{i\hbar}{E-E_0}[G(t) + t_r e^{-iE_0 t/\hbar}K(\tau,E)] \quad (45)$$

with

$$K(\tau,E) = \frac{1}{z(E)} \left[ \frac{e^{-i2\pi y(E)\tau}}{1+\pi v}(e^{-z(E)\tau} - 1) \right.$$

$$\left. + (2\pi)^2 v[\rho Z(\tau) + iy(E)H(\tau,E)] \right], \quad (46)$$

where

$$H(\tau,E) = \sum_{m=1}^{\infty} A_m(\tau) \sum_{j=0}^{m-1} (j+1)!\alpha_j(m)$$

$$\times \left[ D_j(\tau,m) + \frac{1-e^{z(E)(\tau-m)}}{[z(E)]^{j+1}} \right]$$

$$\times \Theta(\tau-m), \quad (47)$$

$$D_j(\tau,m) = \sum_{k=1}^{j} \frac{1}{k!} \frac{(\tau-m)^k}{[z(E)]^{j+1-k}}, \quad D_{j<k}(\tau,m) = 0, \quad (48)$$

and

$$z(E) = 2\pi[\rho - iy(E)],$$

$$y(E) = \frac{E-E_0}{\Delta} = x + \frac{E-E^{(0)}}{\Delta}. \quad (49)$$

The above $G(t)$ and $I(t,E)$, when combined with Eqs. (32)–(34), lead to the final time-dependent amplitudes

$$b_0(\tau) = [e^{-2\pi\rho\tau} + (2\pi)^2 uvZ(\tau)]e^{-iE_0 t/\hbar}, \quad (50)$$

$$b_p(\tau) = 2\pi\sqrt{uv}\,K(\tau,E_p)e^{-iE_0 t/\hbar}, \quad (51)$$

$$b_{E^{(1)}}(\tau) = i2\pi \left[ \frac{V_{E^{(1)}0}}{\Delta} \right] K(\tau,E^{(1)})e^{-iE_0 t/\hbar}, \quad (52)$$

which are fully analytical nonperturbative solution of our $\Lambda$ model with the Bixon-Joertner QC. This solution is nonlinear with respect to the intensities of the two lasers applied, the embedding and the probing ones. After replacing the laser coupling between the QC and the continuum by Coulombic configuration interaction, our solution becomes the solution of the old stated Fano problem of a number of discrete autoionizing states and one continuum [26], but, contrary to the Fano result, with the advantage of no restriction on the probing strength. With our solution we can find the time-dependent ionization probability $P(\tau)$ as

$$P(\tau) = 1 - |b_0(\tau)|^2 - \sum_p |b_p(\tau)|^2. \quad (53)$$

For a fixed laser pulse duration and intensities, we will study this ionization probability as a function of two-photon Raman detuning, i.e., the so-called ionization spectrum. We will also study the dependence of ionization probability on laser intensities, for a fixed time and detuning, pointing to the effect of stabilization, i.e., to a decrease in ionization with increasing intensities.

## III. RESULTS

### A. Weak-probe spectra

First, we shall consider briefly the case usually realized in standard LICS experiments. It is the case of very weak coupling between the ground level and the continuum, to be referred to as the weak-probe case. Mathematically it means that $|u| \ll 1$, with no restriction on $v$. Under this weak-probe condition and for interaction times $\tau$ not exceedingly long, very weak depletion [$\gamma_0 t = 4\pi\tau\,\mathrm{Re}(u) \ll 1$] of the initially populated ground level is expected and all the population probabilities should be linear in $u$. In particular, linear in $u$ probabilities for discrete sates can be obtained from our general Eqs. (50) and (51) by formally setting $u = 0$ in Eqs. (40) and (46) for $Z(\tau)$ and $K(\tau,E_p)$. For $u = 0$, only the first term with $j = 0$ in our Laguerre polynomial is nonzero and amounts to $\alpha_0(m) = m$. As a result $Z(\tau)$ is simply reduced to a geometric series over $m$, combined with first derivative of this series, whose upper limit is determined by the Heaviside function $\Theta(\tau-m)$ and thus equal to $N = \mathrm{Int}(\tau)$. Both this series and its derivative are analytically calculated straightforwardly, giving

$$Z(\tau) \overset{u=0}{=} \frac{1}{4} \left[ \frac{1+\zeta}{1-\zeta_1} \right]^2 [(\tau-N)\zeta_1^{N+1} - (\tau-N-1)\zeta_1^N$$

$$+ (1-\zeta_1)\tau - 1]e^{-i2\pi x}, \quad (54)$$

where $\zeta = (1-\pi v)/(1+\pi v)$ and $\zeta_1 = \zeta\exp(-i2\pi x)$. It is equally simple to calculate $H(\tau,E_p)$ when $u = 0$, obtaining as a result

$$K(\tau,E_p) \overset{u=0}{=} i\frac{1+\zeta}{4\pi(x+p)} \left[ 1-e^{-i2\pi\tau(x+p)} - (1-\zeta)e^{-i2\pi x} \left[ \frac{1-\zeta_1^N}{1-\zeta_1} - \frac{1-\zeta^N}{1-\zeta}e^{-i2\pi(\tau-1)(x+p)} \right] \right]. \quad (55)$$

MULTILEVEL LIGHT-INDUCED CONTINUUM STRUCTURE: ...

Equations (54) and (55) are our previous result in [14], there obtained along a different line, namely, by setting $\gamma_0 = 0$ as early as in Eq. (36) for $F(s)$. By combining the above equations with Eqs. (50), (51), and (53) we have a convenient tool to calculate the ionization probability $P(\tau)$, but in a weak-probe case only. This weak-probe case was studied by us previously [14] in detail. Strictly speaking, we have studied the weak-probe normalized ionization probability $P(\tau)/(\gamma_0 t) = P(\tau)/[4\pi\tau \, \text{Re}(u)]$ against the normalized Fano detuning $\epsilon$ related to our $x$ through $\epsilon = -\{q + [x/\text{Re}(v)]\}$. The main result found was that by the appropriate choice of time, such that the probing $(\gamma_0 t \ll 1)$ and embedding $(\gamma t \gg 1)$ conditions were simultaneously fulfilled, the LICS spectrum was a Fano train, i.e., a series of equidistant asymmetrical profiles with transparent windows and enhancement points, each profile being described by the familiar Fano formula $(q + \epsilon)^2/(1 + \epsilon^2)$ known from the fundamental model of the LICS with only a single excited level instead of a quasicontinuum. Referring the reader to [14] for details on weak-probe multilevel LICS spectra, we now focus our attention on the strong-probe case not discussed so far, when the approximated Eqs. (54) and (55) become invalid.

## B. Strong-probe spectra

Figures 3–5 show the exact spectra, i.e., the ionization probability $P$ versus the normalized Raman detuning $x$, obtained with the use of the exact Eq. (40) for $Z(\tau)$ and the exact Eq. (46) for $K(\tau, E)$. All figures are made for the Fano parameter $q = 1$ and, to save computer time, for a not exceedingly long time $\tau = 30$. For the Rydberg quasicontinuum around the level of the principal quantum number $n = 40$, for which $t_r = 10$ ps, the chosen $\tau$ corresponds to the real time of $t = 300$ ps. Figures 3–5 differ with respect to the choice of the embedding-laser strength $\text{Re}(v)$. We have chosen three strongly dissimilar strengths, namely, $\text{Re}(v) = 10^{-2}$ in the case of Fig. 3 (weak embedding), $\text{Re}(v) = 1/\pi$ in the case of Fig. 4 (moderate embedding), and $\text{Re}(v) = 3$ in the case of Fig. 5 (strong embedding). The second embedding-laser strength is a threshold, one above which the stabilization effect in the quasicontinuum-plus-continuum subsystem starts to play its role [20–23]. When combining these strengths with the assumed time, we find $\gamma t = 4\pi\tau \, \text{Re}(v)$ equal to $1.2\pi$ for Fig. 3, 120 for Fig. 4, and 1130 for Fig. 5. These $\gamma t$ values ensure that the embedding of the quasicontinuum into the continuum is at least partly established. The spectra in each figure have been made for two different probe laser intensities, the one corresponding to weak-probe case $[\text{Re}(u) = 10^{-4}\text{Re}(v)]$ and the other to the strong-probe case $[\text{Re}(u) = \text{Re}(v)]$.

In Fig. 3, $\text{Re}(v) = 10^{-2}$ is assumed, which means that the embedding laser perturbs each level in the quasicontinuum to an extent much smaller than the level spacing $(\hbar\gamma/\Delta = 0.02)$, thus leaving the levels isolated from one another. It is the case of weak embedding. Figure 3(a) is a weak-probe spectrum $[\text{Re}(u) = 10^{-4}\text{Re}(v)$, $\gamma_0 t = 4\pi\tau\text{Re}(u) = 1.2\pi \times 10^{-4}]$ composed, as seen, of a

train of identical, equidistant, asymmetric profiles, well built up around the Raman two-photon resonances with successive levels in the quasicontinuum $(x = 0, \pm 1, \pm 2, \ldots)$. The included asterisk line corresponds to the absence of the embedding laser $[\text{Re}(v) = 0]$ and we see in this case a flat spectrum on the level of $\gamma_0 t = 1.2\pi \times 10^{-4}$. By a comparison of the solid and asterisk lines, both the enhancement point $[P/(\gamma_0 t) > 1]$ and the transparent window $[P/(\gamma_0 t) < 1]$ are seen in each individual profile. Each individual profile, though resembling the Fano profile, is not, however, the exact Fano profile. The
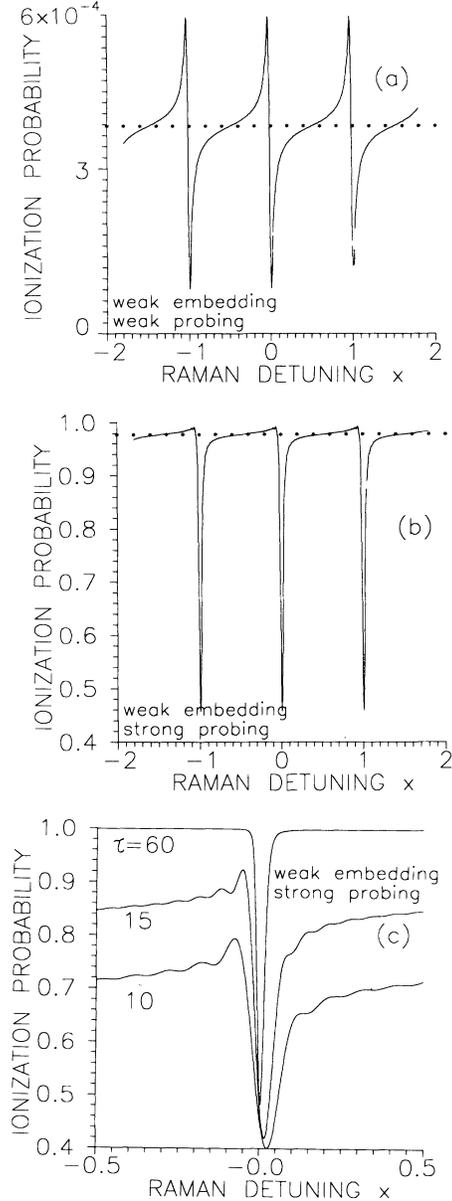


FIG. 3. Part of the multilevel LICS spectrum under the conditions of weak embedding $\text{Re}(v) = 10^{-2}(\hbar\gamma/\Delta = 0.02)$. The other parameters are $q = 1$ and $\tau = 30$. The asterisks correspond to the lack of the embedding laser $\text{Re}(v) = 0$. (a) Weak probe spectrum $[\text{Re}(u) = 10^{-4}\text{Re}(v)]$; (b) strong probe spectrum $[\text{Re}(u) = \text{Re}(v)]$; (c) narrowing of a given dip from (b) with increasing laser-atom interaction time.

reason for this is that the parameters $\mathrm{Re}(u)$ and $\mathrm{Re}(v)$ taken are not dissimilar enough and the time is not sufficiently long for complete embedding to be established (compare Fig. 3 and the analysis in our previous paper [14]). We have observed that with the increase of probe strength each individual profile from Fig. 3(a) became higher and broader and its wings lifted up. In the extreme strong-probe case [Fig. 3(b)], when the probing is as strong as the embedding [$\mathrm{Re}(u) = \mathrm{Re}(v)$, $\gamma_0 t = 1.2\pi$], the wings are lifted so high that in place of asymmetric peaks from Fig. 3(a) we observe dips. The dips are seen to be formed at the positions corresponding to the exact resonant frequencies ($x = 0, \pm 1, \pm 2, \ldots, \pm p$) for Raman transitions from the ground level to the levels in the quasicontinuum. Away of these resonant frequencies the

FIG. 5. Same as in Fig. 3, but for strong embedding $\mathrm{Re}(v) = 3$ ($\hbar\gamma/\Delta = 6$).

FIG. 4. Same as in Fig. 3, but for moderate embedding $\mathrm{Re}(v) = 1/\pi$ ($\hbar\gamma/\Delta = 2/\pi$).

strong-probe spectrum is seen to be nearly saturated ($P \simeq 1$). The dips formed are the result of population trapping [6]. In the long-time scale the trapping is caused by the existence of the purely imaginary pole $s = -iE_0/\hbar$ at resonance frequencies ($E_p = E_0$) in our discrete-level Laplace solutions given by Eqs. (29) and (30). According to Eq. (28), the residuum of $G(s)$ at the pole $s = -iE_0/\hbar$ amounts to $2/[(1+iq)(\gamma_0+\gamma)]$. It leads to the trapping of the following populations by the two resonantly coupled levels after a long time: $|b_0(\infty)|^2 = \gamma^2/(\gamma_0+\gamma)^2$ and $|b_p(\infty)|^2 = \gamma_0\gamma/(\gamma_0+\gamma)^2$. In the strong-probe case ($\gamma_0 = \gamma$), as much as half of the population is predicted by these formulas to be trapped and thus the long-time ionization probability must drop from 1 to 0.5 at resonance frequencies. This is nearly what we see in Fig. 3(b) — the observed ionization slightly lower than 0.5 in the dips means that the time $\tau = 30$ chosen by us cannot yet be considered as long enough. In Fig. 3(c) we show that with increasing laser-atom interaction time, each individual dip from Fig. 3(b) becomes narrower and at the perfectly resonance frequency the ionization tends to 0.5. Such a behavior of our multilevel model is consistent with the predictions of the fundamental model with one excited level exclusively [6,7]. The whole Fig. 3 shows that at weak embedding $\mathrm{Re}(v) = 10^{-2}$, the spectrum evolves from a train of asymmetric peaks to a train of dips, localized at the positions corresponding to the frequencies resonant with Raman transitions from the

ground to quasicontinuum levels.

In Fig. 4 stronger embedding $Re(v)=1/\pi$ is assumed. It means that now the embedding laser broadens each quasicontinuum level to an extent comparable to the quasicontinuum spacing $(\hbar\gamma/\Delta=2/\pi)$. It could be called the moderate embedding case. In this case a given quasicontinuum level is no longer isolated from another one and it generates a qualitatively new situation when compared to the weak embedding case $Re(v)=10^{-2}$. This is the reason why the spectra in Fig. 4 differ form those in Fig. 3. The weak-probe case [Fig. 4(a)], for which $Re(u)=10^{-4}Re(v)$ and $\gamma_0 t=1.2\times10^{-2}$, has a simple interpretation. In this case the spectrum should reflect the dressed-state structure created when strong embedding laser couples the quasicontinuum to the true continuum. Under the assumed weak-probe condition, peaks are thus expected to appear in the spectrum at frequencies ensuring Raman resonances between the ground level and the dressed states created. In the case of the Bixon-Joertner quasicontinuum we have previously [23] derived a closed-form formula allowing us to obtain analytically these dressed-state positions. For $Re(v)=1/\pi$ and $q=1$, the parameters of our interest, this formula, when applied, leads to the following expected resonance peak positions: $x=-0.32+p$, where $p=0,\pm1,\pm2,\pm3,\ldots$. As we see in Fig. 4(a), the peaks formed are in fact localized exactly at the positions predicted by our dressed-state analysis. We observe that with increasing probe strength each peak becomes broader and higher. In the strong probe case [Fig. 4(b)], corresponding to $Re(u)=Re(v)=1/\pi$ and $\gamma_0 t=120$, we observe very broad peaks of the height equal to 1 (saturation) separated by dips. As in Fig. 3(b), each dip is a manifestation of the population trapping in those bare atomic states which are resonantly coupled via two-photon Raman transition. In Fig. 4(c) we show a narrowing of dips with increasing interaction time, as in Fig. 3(c). The whole Fig. 4 shows that the formation of a given peak in the case of moderate embedding $[Re(v)=1/\pi]$ is a collective effect employing all quasicontinuum levels. It stands in difference to the previous case of weak embedding $[Re(v)=10^{-2}]$, when a single asymmetric profile was formed predominantly by a given quasicontinuum level.

Figure 5 corresponds to the strong embedding $Re(v)=3$, when the quasicontinuum-level ionization rate exceeds markedly the level spacing $(\hbar\gamma/\Delta=6)$. The spectra for strong embedding are seen to be formed of peaks, but now localized at $x=-0.47+p$, the positions again agreeing with our dressed-state analysis. There are, however, two noticeable essential differences when one compares them with those for the case of moderate embedding. First, the peaks in the weak-probe spectrum are narrower and second, the peaks in the strong-probe spectrum are lower. The first effect is likely to be related to narrowing of the dressed states, formed in the quasicontinuum-plus-continuum subsystem, with increasing embedding-laser strength. This effect, predicted in [21] and described analytically for the Bixon-Joertner quasicontinuum in [23], does occur for embedding strengths $Re(v)>1/\pi$, for which Fig. 5 is made. On the

other hand, the mentioned peak lowering in the strong-probe case is a manifestation of the stabilization effect in the multilevel LICS, which we are going to consider now.

## C. Stabilization in LICS

As in Figs. 3(b), 4(b), and 5(b) we assume that the ground state and the quasicontinuum are coupled with the same strength to the common continuum by two separate lasers $[Re(u)=Re(v)]$. The intensities of the lasers are assumed to be changed simultaneously and in the same way so that the equality $Re(u)=Re(v)$ is always maintained. Under this condition we calculate from exact Eqs. (53), (51), (50), (46), and (40) the ionization probability versus $Re(u)=Re(v)$, for $q=1$, $\tau=30$, and a fixed Raman detuning $x$. The solid line in Fig. 6 is an exemplifying result obtained for $x=0.5$. We observe that with increasing $Re(u)=Re(v)$ the ionization probability first increases, but after reaching a maximum (saturation), it starts to decrease. Such a decrease in ionization probability with increasing intensity, for a fixed pulse duration, is what is termed stabilization (see [27] for a review). Thus the solid line in Fig. 6 points to stabilization in our multilevel LICS model. To our knowledge, stabilization in the LICS context has not hitherto been considered. It seems that stabilization in the LICS can be understood qualitatively on the basis of some similarities between a limiting case of our multilevel LICS model and the simplest model of Parker and Stroud [28] of Rydberg-atom stabilization. In this simplest stabilization model only a pair of discrete energy-different-levels is coupled with the same strength to a continuum by one laser. In the intensity region determined by the condition that the ionization rate $\gamma$ is greater than the doublet separation $\Delta/\hbar$, this model predicts stabilization due to Raman redistribution via continuum of the initial population in a given level over the two discrete levels (dashed line in Fig. 6). Let us now take the liberty of reducing for a moment the whole quasicontinuum in our multilevel LICS model to a single level. Then, under the assumed condition of
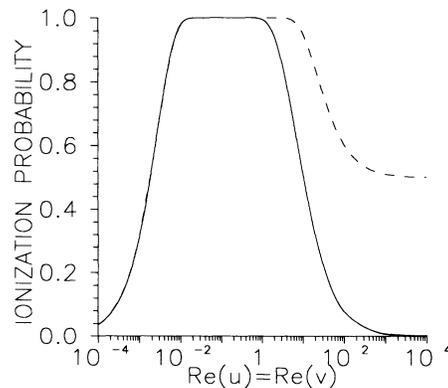


FIG. 6. Ionization probability versus laser intensities under the conditions of $Re(u)=Re(v)$, $q=1$, $\tau=30$, and $x=0.5$. Solid curve, our multilevel LICS model with complete quasicontinuum; dashed curve, the model of Parker and Stroud [28] of a pair of discrete levels equally coupled to the continuum by one laser.

$Re(u) = Re(v)$, our two-laser model with detuning $x$ resembles the one-laser model of Parker and Stroud with level separation equal to $x$. It forms a basis for understanding stabilization in the LICS. Obviously, in our multilevel LICS model with complete quasicontinuum the population redistribution is more complicated because a part of the population transferred to a given quasicontinuum level from the ground level can be further redistributed over whole quasicontinuum by the embedding laser. This is why in the high intensity limit, i.e., for $Re(u) = Re(v) > 1$, the solid curve in Fig. 6, valid for the multilevel LICS model, departs from the dashed curve, valid for the model of Parker and Stroud. The observed fact that in the stabilization region our curve drops well below the curve of Parker and Stroud and tends to zero seems to have a simple explanation, namely, when there is the whole quasicontinuum instead of a single excited level more population has a chance to be trapped in the excited discrete states.

## IV. SUMMARY

In this paper we have solved analytically a general model of light-induced continuum structure in which instead of a single excited level the Bixon-Joertner quasicontinuum of levels was laser embedded into a previously structureless atomic continuum. This multilevel model of the LICS is an optical parallel to the old-stated Fano problem [26] of a number of discrete autoionizing states coupled to the continuum of states by the Coulombic configuration interaction. However, contrary to the Fano result, our solution has the advantage of being fully time dependent (thus applicable to any time scale) and,

moreover, it covers not only the weak-probe case (probing much weaker than the embedding) but all probing strengths up to the strong-probe case (probing as strong as the embedding). With this solution we have considered three physically different cases of the embedding-laser strength, each case determined by the appropriate relation between the quasicontinuum-level ionization rate $\gamma$ and the quasicontinuum spacing $\Delta$, namely, the case of weak embedding ($\hbar\gamma/\Delta \ll 1$), the case of moderate embedding ($\hbar\gamma/\Delta \simeq 1$), and the case of strong embedding ($\hbar\gamma/\Delta \gg 1$). For each embedding-strength case, we have studied the evolution of the ionization spectrum with increasing probe-laser strength. Such strong field effects in the spectra were observed and interpreted as the conversion of a train of asymmetrical Fano-like peaks into a train of dips; peak moving, narrowing and lowering; as well as saturation, population trapping, and stabilization. We have also observed the effect of dip narrowing with increasing laser-atom interaction time. Some of these effects, e.g., a Fano train instead of a single profile, dip train, peak moving and narrowing, as well as complete strong-field stabilization, had their origin in the excited quasicontinuum, which was a part of our multilevel light-induced continuum structure model.

[1] Yu I. Heller and A. K. Popov, Opt. Commun. **18**, 449 (1976).

[2] D. Feldmann, G. Otto, D. Petring, and K. H. Welge, J. Phys. B **19**, 269 (1986).

[3] Bo-nian Dai and P. Lambropoulos, Phys. Rev. A **36**, 5205 (1987).

[4] R. Parzyński, J. Phys. B **20**, 5035 (1987).

[5] Jian Zhang and P. Lambropoulos, Phys. Rev. A **45**, 489 (1992).

[6] M. E. Dutton and B. J. Dalton, J. Mod. Opt. **40**, 123 (1993).

[7] P. L. Knight, M. A. Lauder, and B. J. Dalton, Phys. Rep. **190**, 1 (1990).

[8] Y. L. Shao, D. Charalambidis, C. Fotakis, Jian Zhang, and P. Lambropoulos, Phys. Rev. Lett. **67**, 3669 (1991).

[9] S. Cavalieri, F. S. Pavone, and M. Matera, Phys. Rev. Lett. **67**, 3673 (1991), and unpublished.

[10] O. Faucher, D. Charalambidis, C. Fotakis, Jian Zhang, and P. Lambropoulos, Phys. Rev. Lett. **70**, 3004 (1993).

[11] P. Kristensen, H. Stapelfeldt, P. Balling, T. Andersen, and H. K. Haugen, Phys. Rev. Lett. **71**, 3435 (1993).

[12] J. R. Kukliński, M. Lewenstein, and T. W. Mossberg, Phys. Rev. A **48**, 764 (1993).

[13] R. Parzyński, Phys. Lett. A **130**, 476 (1988).

[14] R. Parzyński, J. Schmidt, and A. Wójcik, J. Opt. Soc. Am. B **11**, 1 (1994).

[15] M. Bixon and J. Joertner, J. Chem. Phys. **48**, 715 (1968).

[16] E. Kyrölä and J. H. Eberly, J. Chem. Phys. **82**, 1841 (1985).

[17] P. M. Radmore, S. Tarzi, and P. L. Knight, J. Mod. Opt. **34**, 587 (1987).

[18] R. Parzyński and A. Wójcik, Acta Phys. Pol. A **78**, 393 (1990).

[19] C. E. Caroll and F. T. Hioe, Phys. Rev. Lett. **68**, 3523 (1992); Phys. Rev. A **47**, 571 (1993).

[20] M. V. Fedorov, M. Yu Ivanov, and A. M. Movsesian, J. Phys. B **23**, 2245S (1990).

[21] M. V. Fedorov and A. M. Movsesian, J. Opt. Soc. Am. B **6**, 928 (1989).

[22] L. Roso-Franco, G. Orriols, and J. H. Eberly, Laser Phys. **2**, 741 (1992).

[23] A. Wójcik and R. Parzyński, Phys. Rev. A **50**, 2475 (1994).

[24] G. C. Stey and W. Gibberd, Physics **60**, 1 (1972).

[25] I. M. Ryzhik and I. S. Gradshteyn, *Tablicy Integralov, Sum, Ryadov i Proizvedeniy* (Nauka, Moscow, 1971), p. 859.

[26] U. Fano, Phys. Rev. **124**, 1866 (1961).

[27] K. Burnett, V. C. Reed, and P. L. Knight, J. Phys. B **26**, 561 (1993).

[28] J. Parker and C. R. Stroud, Jr., Phys. Rev. A **41**, 1602 (1990).